

Stochastic Modeling of GPS Receiver Clocks for Improved Positioning and Fault Detection Performance

Fang-C. Chan and Boris Pervan *Illinois Institute of Technology*

BIOGRAPHY

Dr. Fang-Cheng Chan received his B.S. in mechanical engineering from National Taiwan University, Taipei, Taiwan, in 1991, M.S. in mechanical and aerospace engineering from Illinois Institute of Technology, Chicago, IL, in 2001, and Ph.D. in mechanical and aerospace engineering from Illinois Institute of Technology, Chicago, IL, in 2008. After graduating from college and serving obligated military service, he worked as a mechanical design engineer at Acer Peripherals Inc. (now BenQ Corporation) in Taiwan. He is currently a senior research associate at the NavLab in the department of mechanical and aerospace engineering at the Illinois Institute of Technology, Chicago. Currently he is working on the GPS Evolutionary Architecture Study (GEAS) research. His research interests are GPS, INS and navigation sensor integration, and linear and non-linear optimal estimations.

Dr. Boris Pervan is Associate Professor of Mechanical and Aerospace Engineering at the Illinois Institute of Technology (IIT), where he conducts research on high-integrity satellite navigation systems. Prof. Pervan received his B.S. from the University of Notre Dame, M.S. from the California Institute of Technology, and Ph.D. from Stanford University. Prior to joining the faculty at IIT, he was a spacecraft mission analyst at Hughes Space and Communications Group and was project leader at Stanford University for GPS LAAS research and development. He was the recipient of the Mechanical and Aerospace Dept. Excellence in Research Award (2007), IIT/Sigma Xi Excellence in University Research Award (2005), University Excellence in Teaching Award (2005), Ralph Barnett Mechanical and Aerospace Dept. Outstanding Teaching Award (2002, 2009), IEEE Aerospace and Electronic Systems Society M. Barry Carlton Award (1999), RTCA William E. Jackson Award (1996), Guggenheim Fellowship (Caltech 1987), and Albert J. Zahm Prize in Aeronautics (Notre Dame 1986). He is currently Editor of the ION journal Navigation

ABSTRACT

A multiple-state stochastic clock model of a GPS receiver clock is derived using methods that have been successfully applied in existing models for high-quality satellite clocks. An advantage of having a stochastic receiver clock model is that it can lead to improved positioning performance in GPS navigation systems. Another benefit is that the additional redundancy provided by a clock dynamic model can increase fault detection performance and availability of receiver autonomous integrity monitoring (RAIM).

It is shown that a four-state receiver clock model, which accounts for both the clock's random and deterministic errors, can be easily incorporated into a Kalman filter for improved the real-time position and clock state estimation, without the need for a corresponding dynamic model for the position states. As a preliminary analysis, the results of the estimated receiver clock from the Kalman filter framework is then used to quantitatively evaluate the performance improvements in both positioning (fault-free availability) and fault detection (RAIM availability). In this work, current navigation systems under consideration by the GNSS Evolutionary Architecture Study (GEAS) are used as benchmark applications for performance evaluation using the receiver clock model augmentation.

INTRODUCTION

Precise time information dissemination is the key to the success of Global Positioning System. Therefore, onboard GPS satellite clocks are required to have excellent frequency stability. High quality atomic clocks are the current choice due to their extremely stable frequency over long durations [1-2]. The quality and stability of atomic clocks has been extensively studied [3-4] and the analytical equations for the covariance of clock coasting phase and frequency random errors were mathematically

derived through an impulse response model in [5-6]. This derivation was re-visited by the authors in this current work and the results were validated through actual GPS measurements collected by static GPS receivers. The validated stochastic clock model is able to predict the covariance of high quality atomic clock coasting errors more precisely than a simple slope model. Therefore, the use of a stochastic model can more faithfully predict the performance of any application that involves clock coasting error prediction.

Cost effective commercial GPS receivers have been widely used in a wide variety of services and applications. Low-cost low-stability receiver clocks (such as temperature compensated crystal oscillator, TCXO) can be employed at the expense of requiring one more satellite (minimum four SVs in view) to solve for the receiver clock offset during positioning. For more demanding applications, however, a high quality receiver clock may have great benefits [7], albeit with cost increase that comes with incorporating such a clock in a GPS navigation system. To be able to utilize the benefit of high precision receiver clock and ensure the system integrity simultaneously, the clock phase deviations from GPS time and the frequency deviations from clock nominal frequency have to be estimated reliably. In response, a different four-state clock model for high quality atomic clocks is presented in the paper. The advantages of the four-state clock model over more conventional two-state clock models and least-squares (LS) fit approaches are detailed later in this paper.

Using navigation architectures under consideration by the GNSS Evolutionary Architecture Study (GEAS) [8] as benchmark applications, a preliminary analysis of using high quality receiver clock estimates from a Kalman filter are presented. The results show great potential for performance improvements in the GEAS system availability due to improvement in the position accuracy (mainly in vertical position) and fault detection.

STOCHASTIC CLOCK MODEL

Clock dynamics has been the focus of a great deal of research because of the extensive usage of clocks in various modern electronic devices. The power spectrum of the clock outputs has proved to be a very useful tool to analyze the stability of clock behavior, regardless of the physical realization of the clock. In general, a power law behavior (magnitude proportional to $1/f^\alpha$) can be observed in the power spectrum of clock outputs [9-10]. Table 1 displays the coefficient symbols and the originating sources of clock phase errors [11].

For high quality atomic clocks, phase noise originating from the instability of the phase itself is small and will not accumulate over time. Therefore, the dominant phase-

Table 1 Coefficients of power law model

Symbol of Coefficients	h_2	h_1	h_0	h_{-1}	h_{-2}
Magnitude	$h_2 f^2$	$h_1 f$	h_0	h_{-1}/f	h_{-2}/f^2
Source of Modulation	white phase	flicker phase	white freq.	flicker freq.	random walk freq.

error source is the accumulated error coming from frequency instability (h_0 , h_{-1} and h_{-2}). However, it is difficult to apply a linear model to account for all frequency instabilities for two reasons: first is the flicker noise (h_{-1} term) which cannot be represented using a system model with a rational transfer function of polynomials [12-13]; second is the averaging-over-time effect on the coasting average frequency deviation. Nevertheless, the relationship between the power law coefficients and the covariance of random clock phase and average frequency deviations (two random states) after a certain clock coasting (free-running) period can be derived analytically through impulse response methods. The derivation has been presented in [5] and [6] and is revisited by the authors in the appendix. The results are written below:

$$E([b_{w0} \ b_{w1}]^T [b_{w0} \ b_{w1}]) = \begin{bmatrix} q_{11} & q_{12} \\ q_{21} & q_{22} \end{bmatrix} \quad (1)$$

$$q_{11} = \frac{h_0}{2} \Delta t + 2h_{-1} \Delta t^2 + \frac{2}{3} \pi^2 h_{-2} \Delta t^3$$

$$q_{22} = \frac{h_0}{2\Delta t} + 2h_{-1} + \frac{2}{3} \pi^2 h_{-2} \Delta t$$

$$q_{12} = q_{21} = \frac{h_0}{2} + 2h_{-1} \Delta t + \frac{2}{3} \pi^2 h_{-2} \Delta t^2$$

where b_{w0} is the accumulated clock phase deviation due to the random frequency deviation b_{w1} , and Δt is the clock coasting or free-running time.

The derived stochastic clock coasting error model will be experimentally validated in the next section. In Figure 1, Equation (1) is used to generate the predicted standard deviation (σ) curves of random coasting phase errors for rubidium frequency standards, which are listed in Table 2. The figure also shows the $1-\sigma$ GEAS clock-ephemeris linear coasting error model (8.5×10^{-4} m/sec).

A two-state stochastic model is sufficient to properly model random clock coasting errors for high quality atomic clock, such as commercially available rubidium clocks. (Two additional states will be used to handle deterministic errors, as we will see later in the paper.) For clocks with lower frequency stability, like chip-scale atomic clock (CSAC) [15] or high-end oven-controlled crystal oscillator (OCXO), a three-state stochastic model

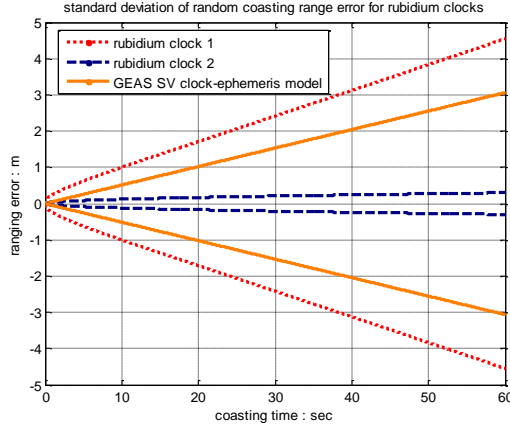


Figure 1 One- σ curves for the two rubidium clock models and the GEAS linear model

is necessary to account for the randomness in frequency drift. A similar methodology to the one explained in the appendix can be used to derive analytical results for the covariance of three-state stochastic clock model. These results will be published in a future paper.

As discussed in the appendix, it is important to clarify that the analytically derived covariance of the clock coasting errors is an average over the coasting period. It does not represent the covariance of instantaneous clock coasting error. This fact will also be important when it comes to implement the stochastic clock error model for receiver clocks.

MODEL VALIDATION USING GPS SATELLITE CLOCKS

Four sets of GPS carrier-phase measurement data from different days were processed to generate the estimated time traces of GPS satellite clock-ephemeris coasting errors. The data was collected by a NovAtel OEM V GPS receiver with an antenna rigidly mounted at a meter-height post on the rooftop of the two-story Engineering-1 building in Illinois Institute of Technology (IIT). During part of the data collection interval, data was also collected by a NovAtel DL-IV GPS receiver on the ground at another site (an empty parking lot) which is about a half mile away from the IIT site. The parking lot data is used as a comparison to prove that the estimated clock-ephemeris traces are dominated by the intended SV clock-ephemeris coasting errors (common for both sites) and not driven by multipath (since the two sites have completely different surrounding environments) or other residual errors.

The observation equations of the GPS carrier-phase measurement for L1 and L2 frequencies are listed below as:

Table 2 Values of the h coefficients from literature and for the proposed model

	h_0	h_{-1}	h_{-2}	reference
rubidium 1	2×10^{-20}	7×10^{-24}	4×10^{-29}	[6]
rubidium 2	5.3×10^{-22}	0	1.2×10^{-31}	[14]
proposed model	2×10^{-21}	0	1.2×10^{-31}	$\sigma_{\text{df}} = 2 \times 10^{-4}$

$$\lambda_1 \phi_{1,k}^i = \rho_k^i + b_{rc,k}^i + b_{sv,k}^i + T_k^i - I_k^i + \lambda_1 N_1^i + m_{1,k}^i + v_1^i \quad (2)$$

$$\lambda_2 \phi_{2,k}^i = \rho_k^i + b_{rc,k}^i + b_{sv,k}^i + T_k^i - I_k^i + \lambda_2 N_2^i + m_{2,k}^i + b_{12}^i + v_2^i \quad (3)$$

where the subscript numbers “1” and “2” are used to indicate L1 and L2 frequencies, subscript k is the time index and superscript i indicates the satellite prn number; λ and ϕ are the carrier wavelength in meters and carrier-phase measurement in cycles respectively; ρ is the true geometry range between the receiver and the satellite; b_{rc} and b_{sv} are receiver clock and satellite clock-ephemeris errors respectively; T and I are the common tropospheric and ionospheric errors; N is the carrier-phase integer ambiguity; m is the carrier-phase multipath; b_{12} is the inter-frequency bias and v is the carrier-phase measurement noise.

An ionosphere-free carrier-phase measurement is formed by pre-multiplying Equation (3) by $f_2^2/(f_1^2 - f_2^2)$ and subtracting it from Equation (2) that is pre-multiplied by $f_1^2/(f_1^2 - f_2^2)$:

$$\begin{aligned} \lambda_w \phi_{w,k}^i &= \frac{f_1^2}{f_1^2 - f_2^2} \lambda_1 \phi_{1,k}^i - \frac{f_2^2}{f_1^2 - f_2^2} \lambda_2 \phi_{2,k}^i \\ &= \rho_k^i + b_{rc,k}^i + b_{sv,k}^i + T_k^i - \frac{f_2^2}{f_1^2 - f_2^2} b_{12}^i \\ &\quad + \lambda_w \left[\frac{f_1}{f_1 + f_2} N_1^i - \frac{f_2}{f_1 + f_2} N_2^i \right] \\ &\quad + \frac{f_1^2}{f_1^2 - f_2^2} m_{1,k}^i - \frac{f_2^2}{f_1^2 - f_2^2} m_{2,k}^i + v_{w,k}^i \\ \lambda_w &= c/(f_1 - f_2) \end{aligned} \quad (4)$$

where c is the speed of light and v_w is the ionosphere-free carrier-phase measurement noise.

Taking a time differences on the ionosphere-free carrier-phase measurements in Equation (4) with respect to an arbitrary starting time t_0 , time invariant components, such

as integer ambiguities and inter-frequency bias, are eliminated:

$$\begin{aligned}
\lambda_w \phi_{w,k-0}^i &= \lambda_w \phi_{w,k}^i - \lambda_w \phi_{w,0}^i \\
&= \rho_{k-0}^i + b_{rc,k-0}^i + b_{sv,k-0}^i + T_{k-0}^i \\
&\quad + \frac{f_1^2}{f_1^2 - f_2^2} m_{1,k-0}^i - \frac{f_2^2}{f_1^2 - f_2^2} m_{2,k-0}^i + v_{w,k-0}^i
\end{aligned} \quad (5)$$

With multiple common satellites in view during the data collection period, one more measurement difference between a pair of satellites is taken to eliminate common receiver clock errors (the same SV clock type was used when selecting the satellite pairs):

$$\begin{aligned}
\lambda_w \phi_{w,k-0}^{i-j} &= \lambda_w \phi_{w,k-0}^i - \lambda_w \phi_{w,k-0}^j \\
&= \rho_{k-0}^{i-j} + b_{sv,k-0}^{i-j} + T_{k-0}^{i-j} + \frac{f_1^2}{f_1^2 - f_2^2} m_{1,k-0}^{i-j} \\
&\quad - \frac{f_2^2}{f_1^2 - f_2^2} m_{2,k-0}^{i-j} + v_{w,k-0}^{i-j}
\end{aligned} \quad (6)$$

The double-difference geometric range, $\hat{\rho}_{k-0}^{i-j}$, is estimated using the pre-surveying site location and satellite broadcast ephemeris. The Wide Area Augmentation System (WAAS) troposphere correction \hat{T}_{k-0}^{i-j} [16] is applied to remove the majority of the tropospheric error. What remains is an estimate of the total clock-ephemeris coasting errors for a pair of GPS satellites:

$$\begin{aligned}
\hat{b}_{sv,k-0}^{i-j} &= \lambda_w \phi_{w,k-0}^{i-j} - \hat{\rho}_{k-0}^{i-j} - \hat{T}_{k-0}^{i-j} \\
&= b_{sv,k-0}^{i-j} + \frac{f_1^2}{f_1^2 - f_2^2} m_{1,k-0}^{i-j} - \frac{f_2^2}{f_1^2 - f_2^2} m_{2,k-0}^{i-j} \\
&\quad + \delta \rho_{k-0}^{i-j} + \delta T_{k-0}^{i-j} + v_{w,k-0}^{i-j}
\end{aligned} \quad (7)$$

As expressed in Equation (7), the quality of the total coasting error estimate for each satellite pair depends on the double-difference range and troposphere model errors, as well as the multipath environment. The similar process to estimate satellite clock errors can be found in [17] for precise standalone GPS positioning.

Figure 2 shows the results from processing the collected data through equations (2)-(7) from the two sites. The nearly identical results for the corresponding SV pairs from two sites demonstrate that the measurement noise and multipath errors have negligible effect on the estimate of the satellite clock-ephemeris coasting errors.

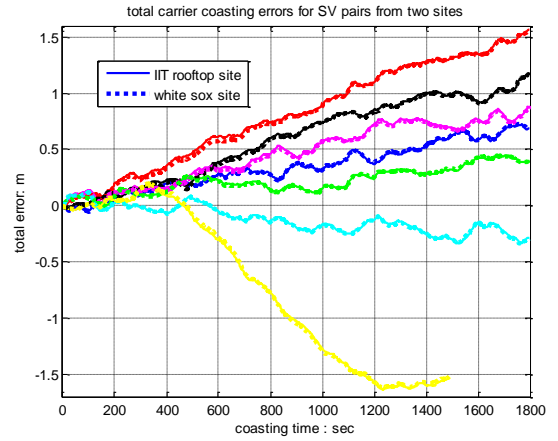


Figure 2 Total SV clock-ephemeris coasting errors from two sites

Residual errors in the double-difference range estimations, $\delta \rho_{k-0}^{i-j}$, can be due to two factors: errors in knowledge of the receiver antenna and satellite positions. The individual positions of the antennas at each of the two sites were estimated using dual-frequency carrier-phase DGPS techniques with the “kar7” CORS site as the reference station, which is about 5 km away from both antenna locations. The standard deviations for horizontal and vertical position errors are expected to be less than 10 cm and 15 cm, respectively. The satellite positions were propagated using broadcast ephemeris. According to GPS Standard Positioning Service (SPS) [18], an RMS User Range Error (URE) is expected to be less than 6 m across the entire constellation over any 24-hour interval. However, the majority of initial ephemeris errors are cancelled out due to time-differential process in Equation (5). Only the change in ephemeris errors impacts the total satellite clock-ephemeris coasting error observables, and the effect is negligibly small. As previously noted, tropospheric delay is corrected by using WAAS tropospheric model. In an effort to reduce the magnitude of tropospheric residuals, only carrier-phase measurements from satellites with at least 30 degree elevation angle were used. According to WAAS Minimum Operational Performance Standards (MPOS) [16], the standard deviation of tropospheric residual after applying WAAS correction is from 25 to 12 cm for 30 to 90 degree elevation angles. Again, the effect of the tropospheric residuals in the double-difference carrier-phase observables is expected to be much less than this because the time-difference process effectively eliminates the initial tropospheric residual biases. Only the residual small drifts during the coasting time can affect the estimation. These are expected to be at the level of a few centimeters at most.

The random parts of the coasting errors for each satellite clock pair were extracted by detrending the slopes from the total coasting errors (to be explained in detail below). The random error estimations are shown in Figures 3 and

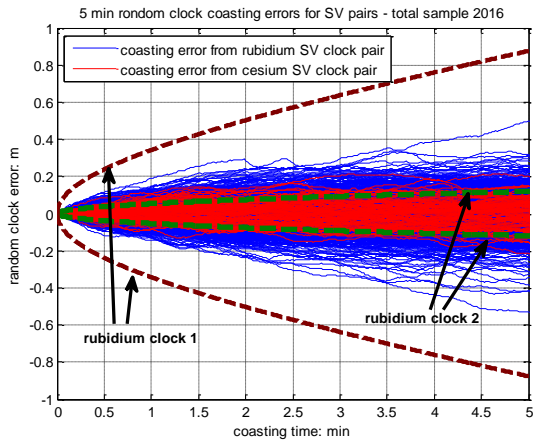


Figure 3 Five-minute random clock coasting errors

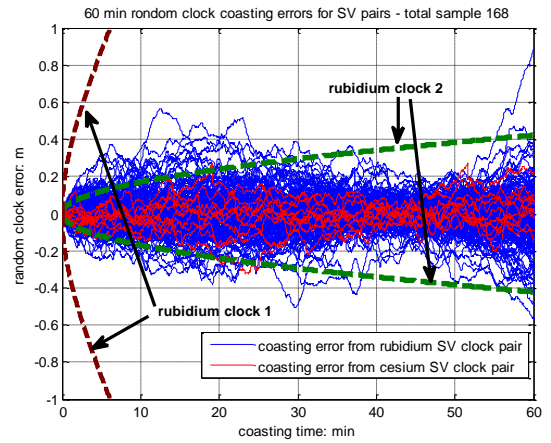


Figure 4 One-hour random clock coasting errors

4 for 5-minute and 1-hour coasting times. Also shown in the figures are the predicting standard deviation curves of the coasting phase errors from the derived stochastic models (scaled by square root of two because the data is for a pair of SV clock) using the rubidium specifications that are listed in Table 2. Both figures illustrate that the predictions from the models fit the growing trend of the random coasting errors, but miss matching the magnitude (the rubidium 1 model is over-conservative while the rubidium 2 model is slightly under-conservative). The results demonstrate that the derived stochastic model is applicable to satellite random coasting errors; however, accurate power law spectrum coefficients for current onboard GPS clocks are difficult to identify, since most of the research on GPS satellite clock stability has focused on long term stability in days, months or even years [1-2], [19]. Therefore, in this work, a set of h coefficients are proposed based on the specifications for rubidium atomic clocks from the literature and the estimated random clock coasting errors in Figures 3 and 4. The proposed h coefficients are intended to function as a start for a standard satellite clock random coasting error model that is adequately conservative for current or future GPS

satellites. The literature-based and proposed h coefficients are listed in Table 2.

The detrended slopes from the estimated total clock-ephemeris coasting errors were obtained by applying LS fit process to fit a straight line into each one-hour long segment of data. The slope physically includes the initial satellite clock frequency bias and the change of ephemeris orbit error. A linear fit model for one hour coasting interval is reasonable to represent non-random (deterministic) clock-plus-ephemeris errors because of two facts: GPS satellite clock correction model is usually linear for 2 hours (a_2 coefficient is always zero and broadcast navigation data is normally updated for every 2 hours), and one-hour straight line is a good approximation for normal satellite orbit errors, which have a 12-hour period.

A histogram of computed LS slopes is shown in Figure 5 with 168 one-hour samples. Although this is not statistically a sufficient sample size to draw firm conclusions about the standard deviation of the clock-ephemeris error rate for a deterministic linear model, it provides a range where we can start with. Similarly, Figures 6-7 show the histograms of clock random coasting errors at coasting times of 5, 15, 30 and 60 minutes. To accommodate both effects, we propose a four-state total clock-ephemeris error coasting model. This model includes two state vectors, \vec{b}_w and \vec{b}_d . The vector \vec{b}_w accounts for the stochastic clock coasting errors with proposed h coefficients listed at the last row in Table 2. On the other hand, the deterministic two-state vector \vec{b}_d behaves linearly. The standard deviation of the predicted total clock-ephemeris coasting errors is the root-sum-square (RSS) of the phase variance from linearly propagating deterministic states and the phase variance that was analytically derived by stochastic model. The discrete-time dynamics of the proposed four-state model

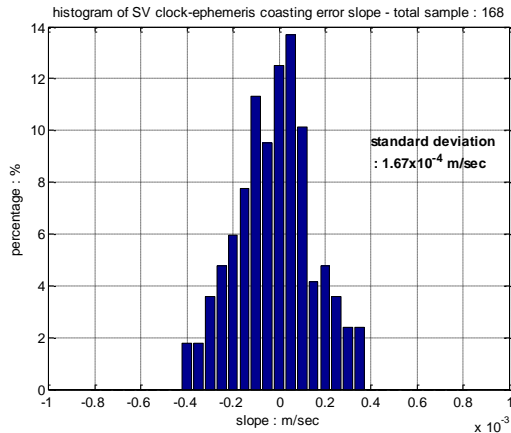


Figure 5 Histogram of detrended slopes

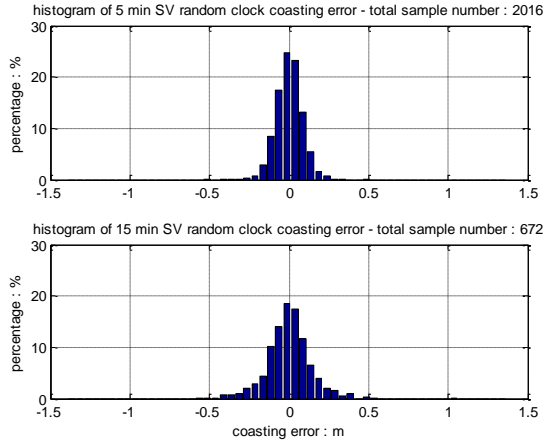


Figure 6 Histograms of SV random clock coasting errors for 5 and 15-minute coasting times

and the total phase coasting error observation model are described in equations (8) - (10):

$$\begin{bmatrix} \bar{b}_{d0} \\ \bar{b}_{d1} \\ \bar{b}_{w0} \\ \bar{b}_{w1} \end{bmatrix}_{t_k} = \begin{bmatrix} 1 & \Delta t & 0 & 0 \\ 0 & 1 & 0 & 0 \\ 0 & 0 & 1 & 0 \\ 0 & 0 & 0 & 1 \end{bmatrix} \begin{bmatrix} \hat{b}_{d0} \\ \hat{b}_{d1} \\ \hat{b}_{w0} \\ \hat{b}_{w1} \end{bmatrix}_{t_0} + \begin{bmatrix} 0 \\ 0 \\ w_0 \\ w_1 \end{bmatrix}_{t_0 \rightarrow t_k} \quad (8)$$

$$\text{where } E \left[\begin{bmatrix} w_0 & w_1 \end{bmatrix}^T \begin{bmatrix} w_0 \\ w_1 \end{bmatrix} \right] = \begin{bmatrix} q_{11} & q_{12} \\ q_{21} & q_{22} \end{bmatrix}_{t_0 \rightarrow t_k} \quad (9)$$

$$\hat{b}_{total,t_k} = \begin{bmatrix} 1 & 0 & 1 & 0 \end{bmatrix} \begin{bmatrix} b_{d0} \\ b_{d1} \\ b_{w0} \\ b_{w1} \end{bmatrix}_{t_k} \quad (10)$$

In predicting coasting error, the initial variances of deterministic phase, \hat{b}_{d0} , and random states, \hat{b}_{w0} and

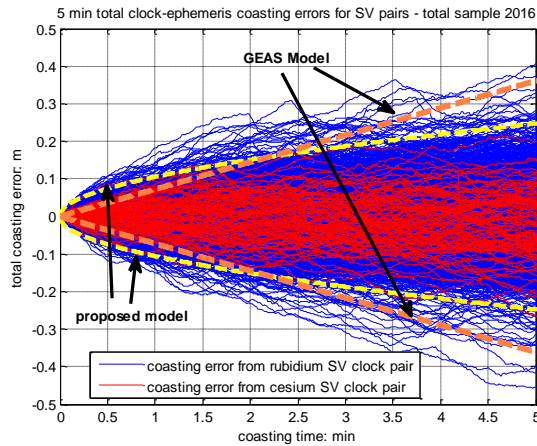


Figure 8 Five-minute total clock-ephemeris coasting errors

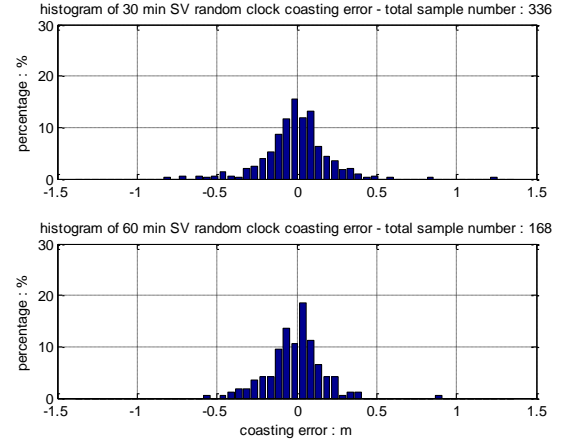


Figure 7 Histograms of SV random clock coasting errors for 30 and 60-minute coasting times

\hat{b}_{w1} , are all set to zero. The stochastic properties of the random states are realized by adding the random process noise in Equation (8). Remember that the covariance of the process noise in Equation (9) can be evaluated by Equation (1) as a function of coasting time. The proposed standard deviation of the deterministic clock-ephemeris error rate is 2×10^{-4} m/sec. There is an important point to note in using the four-state model to predict the standard deviation of the coasting errors. Because of the fundamentally non-linear nature of the model of the two random states, the covariance of the random states must be evaluated using coasting time, which always starts from t_0 . It cannot be evaluated like other linear models that propagate the covariance incrementally within the coasting interval, but only over intended whole coasting period. However, if a measurement was brought in to estimate the states, then the starting time of next coasting period can be set to the time of current measurement update. In this case, the random state covariance can perform sequential propagations like a normal Kalman filter. More details on this idea will be described in the next section.

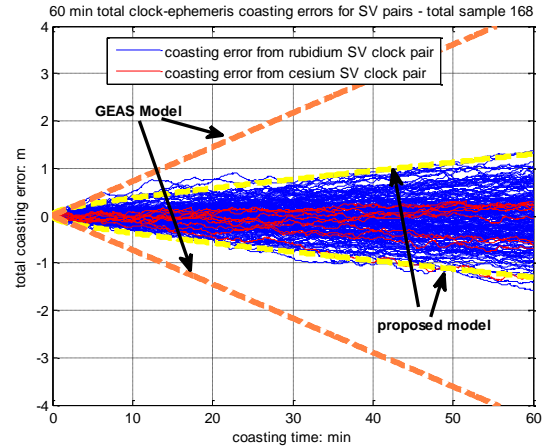


Figure 9 One-hour total clock-ephemeris coasting errors

Demonstration of the validity of the proposed model is best done by using the total coasting errors, rather than random coasting errors alone. This is true because the long term trends of random clock coasting errors might be removed when the coasting errors were de-trended by LS-fit slopes. Figures 8-9 show 5 minutes and 1 hour of total clock-ephemeris coasting errors respectively, and the standard deviation envelopes from both the current GEAS model and the proposed four-state model. Figure 8 shows that the GEAS linear model is less conservative than the proposed four-state model for coasting times less than two minutes. On the other hand, Figure 9 illustrates that for one-hour coasting time, the GEAS linear model is too conservative to make the GEAS model really useful. In summary, the proposed four-state model captures the fast growing phase errors for short coasting times, and yet has a reasonable prediction on total coasting errors for long coasting times. This advantage over a simple linear coasting error model has a significant impact on the performance of applications that concern modeling clock-ephemeris coasting errors, such as Relative RAIM (RRAIM) [8].

KALMAN FILTER IMPLEMENTATION OF FOUR-STATE CLOCK MODEL FOR RECEIVER CLOCK

Clock error estimation has invoked a great deal of research, most of which are taking advantage of Allen variance to estimate the deterministic clock error model [20-21]. This approach is usually good for off-line processing but difficult to implement in real-time estimation. One popular technique for real-time clock error estimation is to use least squares fit process to fit a linear or quadratic model. Then the residuals of the least squared fit model are used as an index of estimation quality [22-23]. However, the covariance of the resulting frequency deviation estimation is too optimistic because the time correlation of random clock errors are not accounted for (they are treated as white noise in general).

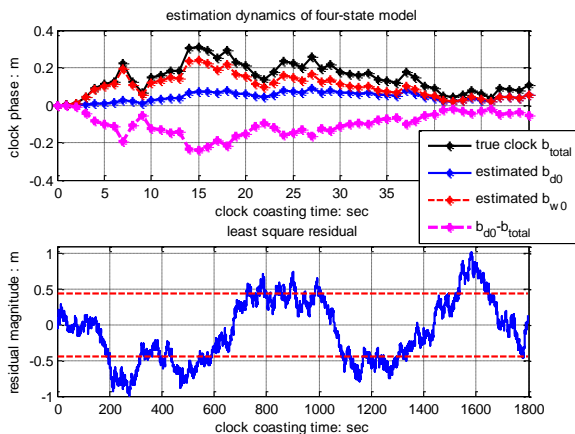


Figure 11 Simulated clock estimation and LS estimation residuals

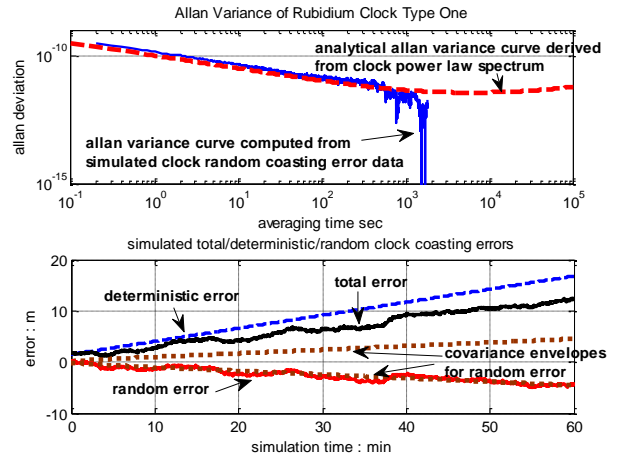


Figure 10 Clock error simulation

A Kalman filter approach, which is equivalent to the batched least-squares process, has also been suggested with intentionally magnified measurement noise to remedy the problem [6]. However, this remedy is not statistically robust. Therefore, the resulting covariance can only be treated as an approximation and be handled on a case by case basis. In contrast, using the validated four-state clock model in a Kalman filter can resolve these problems.

The main advantage of the four-state model, provided that the stochastic clock error model is faithful, is that it can give reliable covariance estimations on both the phase and frequency deviations. The implementation of Kalman filter is otherwise straightforward, using the clock discrete-time dynamics from Equation (8) and the observation matrix from Equation (10). The covariance of the random process noise has to be calculated according to Equation (1) with the coasting time equal to the measurement update interval.

To further understand how the four-state model works, a

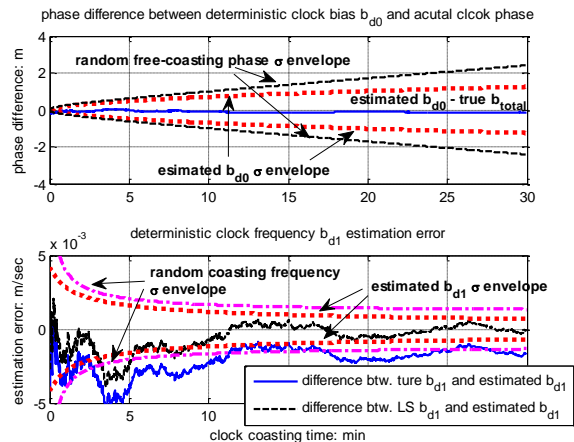


Figure 12 Simulated clock phase and frequency estimation

simple numerical simulation is performed, with results shown in Figures 10-13. In this simulation, discrete-time clock phase coasting errors was numerically simulated using a fractional integration method [24] with the power law spectrum specification for rubidium clock 1 (Table 2). The simulation assumes that the direct clock measurements, with additive white noise, are available every second. The top half of Figure 10 shows that the simulated random clock coasting errors have Allan variance values that are very close to the analytical Allan variance values derived from the adopted h coefficients [11]. This simply shows that the simulated sequences of random clock coasting errors meet the power law spectrum specification adopted for the simulation. The bottom half of Figure 10 shows the 1-hour simulated sequences of total, deterministic, and random clock coasting errors, as well as the variance of the random clock coasting errors. The initial phase and frequency deviations for the deterministic clock states are 1.5 m and 4.25×10^{-3} m/sec respectively (the initial frequency deviation is 5 times greater than the GEAS model 1- σ value). A white measurement noise of 2 mm standard deviation is used.

The variation of the estimated clock phase states, \hat{b}_{d0} and \hat{b}_{w0} , are shown in the top half of Figure 11 together with the true clock phases during the first 50 seconds of the estimation process (the initial true clock phase bias, 1.5 m, has been removed in the figure from the estimated deterministic clock phases and true clock phases for easier illustration). It is clear that the fast changes of the true clock phases are absorbed by the random phase state, to allow a more resembling in smoother behavior of the deterministic phase state. The amount of the absorption by the random phase state is determined by the random state covariance generated by Equation (1). The bottom curve in the top half figure is the difference between the estimated deterministic phase and the true clock phase, which has almost the same value but opposite sign of the estimated random phase. The bottom half of Figure 11 is the LS residuals after fitting a straight line into a 30-minute data set of simulated total clock coasting errors. It indicates the performance of LS estimation process.

The estimation performance of the four-state model is shown in Figure 12. The bottom half of Figure 12 shows the difference between the estimated deterministic frequency \hat{b}_{d1} and the true frequency offset, and that between \hat{b}_{d1} and the LS fitted phase slope. Both of them are converging and stay closely to the covariance envelopes. However, it is obvious that the estimated deterministic frequency is more closely resembles the LS slope value rather than the true frequency offset (the difference is smaller). This is understandable by looking back at the simulated sequence of random clock coasting errors in the bottom half of Figure 10. There is a long

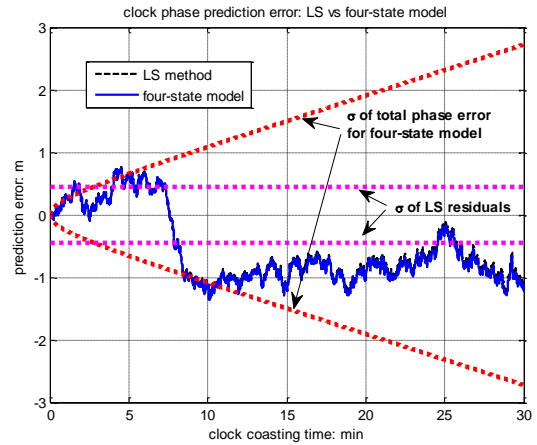


Figure 13 Simulated clock prediction

term, nearly-linear variation buried in the random coasting error sequence. Therefore, the LS fit process and the Kalman filter with four-state clock model both have “observed” the trend and were trying to estimate it. The deterministic phase estimation in the top half of Figure 12 shows an interesting property: the standard deviation of deterministic phase state is not converging but gradually growing (similar to the trend of clock free-coasting errors). However, this is also comprehensible by looking back to the estimation dynamics shown in the top half of Figure 11. In that figure, the random state b_{w0} only absorbs random coasting errors during the short coasting time between measurement updates. In contrast, the deterministic state b_{d0} follows the long term trend of the total coasting errors (random plus deterministic errors). Given that the standard deviation of the total coasting errors is growing over coasting time and the filter can only observe the sum of the random and the deterministic phase states, the uncertainty of the deterministic phase is resulted from the combination of the uncertainty of the total coasting error and the correlation to the random state.

The last figure in this section, Figure 13 shows the 30-min prediction performance from both the LS process and the four-state model after 30-min period of estimation. The actual values of prediction errors from both models are very close (less than 0.1 m difference). However, the predicted standard deviations of the prediction error are quite different. The LS prediction errors grow up to twice the value of the standard deviation of the estimation residual after first 10 minutes. The four-state model, on the other hand, predicts standard deviations reasonably for the first 20 minutes and then becomes over-conservative. Although Figure 13 is only one simulation case, it has clearly showed the lack of effective ways to model the prediction quality for the LS process, which is a serious issue for high integrity systems.

APPLICATION FOR GEAS

GEAS is exploring navigation architectures and performance using modernized GPS dual-frequency (L1/L5) measurements to meet LPV-200 requirements worldwide in 2020 time frame. The details of the LPV-200 requirements can be found in [8]. Several satellite constellations are also considered by GEAS. The numbers of satellites in these constellations are 24, 24 minus 1, 27, 27 minus 1, 30 and 30 minus 1. A validated four-state atomic clock model can help improve the GEAS system performance in different aspects. One is using the four-state model to predict clock-ephemeris coasting errors, instead of using the current GEAS linear model. Better prediction performance can be expected (as shown in Figure 9), especially for the coasting periods which are longer than 10 minutes.

In this work, another aspect of using the four-state clock model to improve GEAS system performance is studied: using the four-state atomic receiver clock model for improved positioning and fault detection. As a preliminary analysis, receiver clock estimation and clock aiding positioning and fault detection are performed as two separate processes. Receiver clock estimations are passed to the positioning and fault detection functions for GEAS Absolute RAIM (ARAIM) architecture [8]. Receiver clock estimation was performed by a standalone GPS filter using ionosphere-free smoothed code (consistent with the GEAS architecture and assumptions) and carrier-phase measurements with the smoothing time of 100 seconds. The four-state atomic receiver clock model was assumed to have the same performance as the rubidium clock 1 (as shown in Table 2). An initial receiver clock frequency offset of 4.25×10^{-3} m/sec (standard deviation) and 30-minute estimation time were used. The initial uncertainties for position and clock phase are setup as a large number. Standalone WAAS tropospheric error models and the proposed clock-ephemeris coasting error model were also included in the filter.

Some simplifications were made in this preliminary analysis in order to reduce the simulation time. Five 30-minute filtering covariance analyses, spreading over 24-

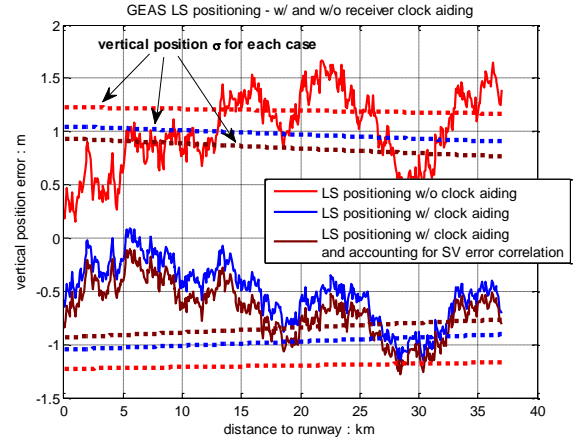


Figure 14 Simulated positioning with and without clock aiding

hour, using the Do-229D constellation [16] were performed. The worst estimation performance for receiver clock phase and frequency deviations were then selected in a look-up table as a function of the number of SV in view seen in Table 3. The quality of the clock aiding were provided by using the four-state clock model with deterministic phase and frequency covariance initialized by checking the look-up table according to the number of satellite in view in the current simulated geometry, plus the random coasting errors evaluated by Equation (1). In principle, the receiver clock estimation error is correlated with other measurement error sources that affect positioning, mainly the satellite clock-ephemeris error. However, for simplicity, this correlation was neglected. This is a conservative action because the correlated measurement errors (the predicting receiver clock measurements and the smoothed code measurement errors from satellite clocks) were treated as independent errors. Figure 14 demonstrates one example of the LS vertical positioning performance of GEAS only, GEAS with simplified clock aiding and the clock aiding that takes into account of the correlation by numerical simulation. It confirms the assertion that neglecting the correlation is conservative because smaller standard deviations of vertical position errors are observed when the correlation is taken into account.

Vertical performance using a optimal multiple hypotheses solution separation algorithm, disseminated in [26], with and without clock aiding is presented as global coverage of fault-free availability (H_0 hypothesis) achieving 95%, 99% and 99.5%. Global site selection is done using 5-degree grid with latitude range from -75 degree to 75 degree. All ARAIM parameters are consistent with the current GEAS ARAIM architecture [8]. It turns out that the performance improvements for positioning and ARAIM fault detection are the same. Therefore, Figure 15-19 show the performance improvements applicable to both positioning and ARAIM detection. The results for

Table 3 Clock estimation performance look-up table

Number of SV in view	σ of b_{d0} (m)	σ of b_{d1} (m/sec)
8 and above	0.9	7.9×10^{-4}
7	0.96	8.1×10^{-4}
6	1.3	8.7×10^{-4}
5	1.7	10×10^{-4}
4	2.0	11.4×10^{-4}

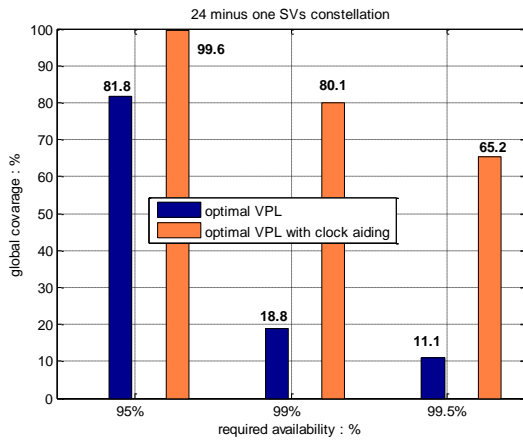


Figure 15 Clock aiding performance for 24-1 SVs constellation

the 24-minus-1-satellite and 24-satellite constellations considered by GEAS are shown in figures 15 and 16.

In Figure 15, significant improvements can be seen for 99% and 99.5% availability requirements with clock aiding. Figure 16 shows here are also encouraging, in that the global coverage increases considerably with receiver clock aiding.

The same simulations are repeated for other constellations that are under consideration in GEAS. The results are shown in Figures 17-19. In general, receiver clock aiding is more helpful when the satellite geometry is not good. For a constellation of 30 SVs (also considered by GEAS), there is no availability gain from receiver clock aiding for positioning or fault detection. Those results, therefore, are not shown here.

SUMMARY AND FUTURE WORK

The derivation of a two-state stochastic model for high quality atomic clock was revisited and it has been shown

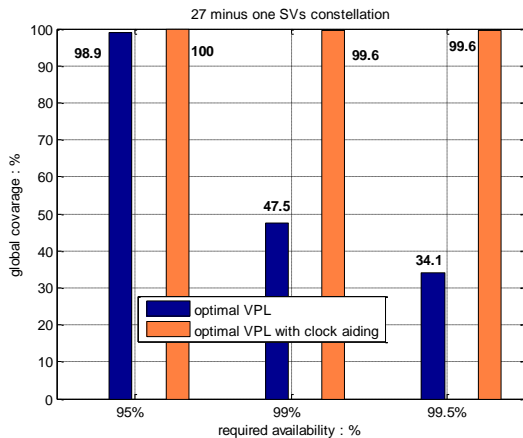


Figure 17 Clock aiding performance for 27-1 SVs constellation

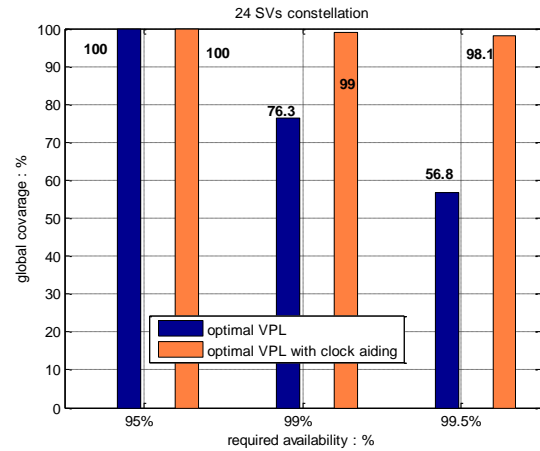


Figure 16 Clock aiding performance for 24 SVs constellation

experimentally that it can be applicable to GPS clock random coasting errors. A different way to utilize the stochastic model was proposed, and using a four-state implementation was introduced and validated experimentally using GPS SV clock data.

A Kalman filter implementation of the proposed four-state model for atomic receiver clock aiding was described in detail, and a simple numerical simulation illustrated the estimation mechanism and the model's effectiveness.

In addition, a preliminary analysis of using the four-state atomic receiver clock model for GEAS applications has been performed. The results illustrate that the receiver clock aiding has the potential to improve the system performance, in term of global coverage. The benefits of receiver clock aiding were evident on both positioning and fault detection for the future GPS satellite constellations which have fewer than 30 SVs.

For atomic clocks which have less frequency stability

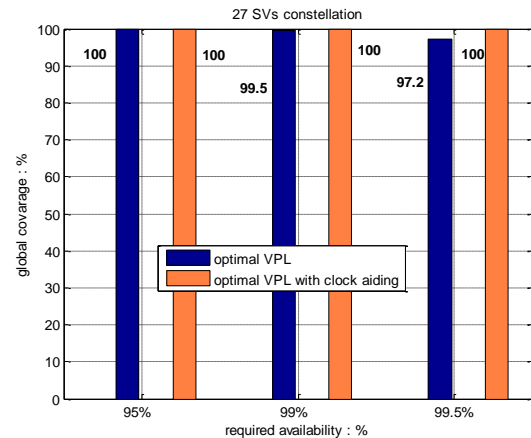


Figure 18 Clock aiding performance for 27 SVs constellation

(such as chip-scale atomic clock or high end OCXO), three-state stochastic models need to be developed using the same methodology that is presented in this paper. As a result, a six-state clock model can be implemented in a Kalman filter without any difficulty. This work is underway and its estimation performance will be presented in a future paper.

To use receiver clock aiding for high integrity applications, the integrity of the clock estimation has to be addressed. A high integrity receiver clock estimator must be developed to address this concern in the future. Due to the correlation between the GPS satellite clock-ephemeris errors and the receiver clock estimation errors, receiver clock aiding for DGPS applications will also be considered. The performance improvement for relative positioning and RRAIM fault detection with clock aiding will be evaluated as well.

ACKNOWLEDGMENTS

The authors would like to thank to the FAA satellite navigation program office for supporting this research. The authors also would like to express their appreciations to Dr. Samer Khanafseh for his peer review and comments, as well as other comments from the colleagues in IIT NavLab.

Disclaimer: The contents of this paper express the views of the authors alone, and they do not necessarily represent the position of any other organization or person.

REFERENCES

[1] Oaks, J., Senior, K., Largay, M., Beard, R. and Buisson, J., "NRL Analysis of GPS On-Orbit Clocks," *Proceedings of the 2005 IEEE International Frequency Control Symposium and Exposition*, 2005

[2] Howe, D. Beard, R. Greenhall, C. and Riley, W., "Enhancements to GPS Operations and Clock Evaluations Using a Total Hadamard Deviation" *IEEE Transactions on Ultrasonics, Ferroelectrics, and Frequency Control*, Vol. 52, No. 8, August 2005

[3] *NIST Technical Note 1337*, National Institute of Standards and Technology, 1990.

[4] Allan, D. W., "Time and Frequency (Time-Domain) Characterization, Estimation, and Prediction of Precision clocks and Oscillators," *IEEE Transactions on Ultrasonics, Ferroelectrics, and Frequency Control*, Vol. UFFC-34, No. 6, November 1987

[5] Van Dierendonck, A. J. and Brown, R. G., "Relationship between Allan Variances and Kalman Filter Parameters," *Proceedings of the Precise Time and Time Interval (PTTI) Systems and Applications*, Category 5, Vol. 29.

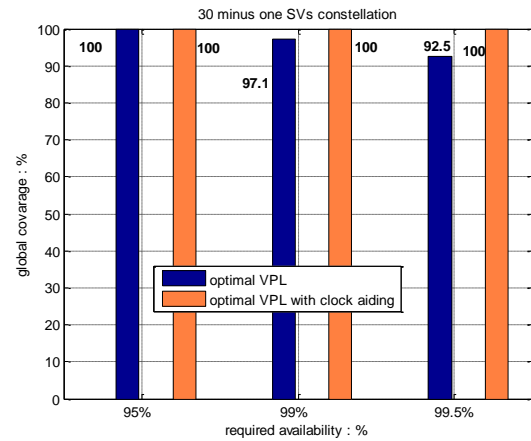


Figure 19 Clock aiding performance for 30-1 SVs constellation

[6] Brown, R. G. and Hwang, P. Y. C., *Introduction to Random Signals and Applied Kalman Filtering*, John Wiley & Sons, New York.

[7] Misra, P., Pratt, M., Burke, B. and Ferranti, R., "Adaptive Modeling of Receiver Clock for Meter-Level DGPS Vertical Positioning," *Proceedings of the ION GPS-95*, Palm Springs, CA, September 1995.

[8] Walter, T., Enge, P., Blanch, J. and Pervan, B., "Worldwide Vertical Guidance of Aircraft Based on Modernized GPS and New Integrity Augmentations" *Proceedings of the IEEE*, Vol. 96, Issue 12, Dec. 2008

[9] Barnes, J. A., et al., "Characterization of Frequency Stability," *IEEE Transactions on Instrumentation and Measurement*, Vol. IM-20, No. 2, May 1971

[10] Rutman, J., "Characterization of Phase and Frequency Stabilities in Precision Frequency Sources: Fifteen Years of Progress," *Proceedings of the IEEE*, Vol. 66, No 9, Sep. 1978

[11] IEEE Std 1139-1999, *IEEE Standard Definitions of Physical Quantities for Fundamental Frequency and Time Metrology-Random Instabilities*, Annex B

[12] Walls, F. L., Feme-Pikal, E. S. and Jefferts, S. R., "The Origin of 1/f PM and AM Noise in Bipolar Junction Transistor Amplifiers," *Proceedings of the 2005 IEEE International Frequency Control Symposium and Exposition*, pp. 294-304, May 1995.

[13] Galliou, S., Sthal, F. and Mourey M., "New Phase-Noise Model for Crystal Oscillators: Application to the Clapp Oscillator," *IEEE Transactions on Ultrasonics, Ferroelectrics, and Frequency Control*, Vol. 50, No. 11, November 2003.

[14] Vernotte, F., Delporte, J., Brunet, M. and Tournier, T., "Uncertainties of drift coefficients and extrapolation errors: Application to clock error prediction," *Metrologia*, Vol. 38, No. 4, 2001.

[15] Knappe, S., et al., "A Chip-scale Atomic Clock Based on Rb-87 with Improved Frequency Stability," *Optics Express*, 13, 1249-1253, 2005.

- [16] RTCA Special Committee 159 Working Group 2, "Minimum Operational Performance Standards for Global Positioning System / Wide Area Augmentation System Airborne Equipment," RTCA Document Number DO-229D, December 2006
- [17] Han, S.-C. Kwon, J. H. and Jekeli, C., "Accurate Absolute GPS Positioning through Satellite Clock Error Estimation," *Journal of Geodesy*, 75: 33-43, 2001.
- [18] "Global Positioning System Standard Positioning Service Performance Standard", Department of Defense, 2001.
- [19] Oaks, J., Largay, M., Reid, W. and Buisson, J., "Global Positioning System Constellation Clock Performance," *Proceedings of the 34th Annual Precise Time and Time Interval (PTTI) Systems and Applications Meeting*, 2002.
- [20] Greenhall, C. A., "The Third-Difference Approach to Modified Allan Variance," *IEEE Transactions on Instrumentation and Measurement*, Vol. 46, No. 3, June 1997.
- [21] Vernotte, F. and Vincent, M., "Relationships between Drift Coefficient Uncertainties and Noise Levels: Application to Time Error Prediction," *Proceedings of the 29th Annual Precise Time and Time Interval (PTTI)*, 1997.
- [22] Misra, P., Pratt, M., Muchnik, R. and Manganis, B., "A General RAIM Algorithm Based on Receiver Clock," *Proceedings of the ION GPS-95*, Palm Springs, CA, September 1995
- [23] Bednarz, S. and Misra, P., "Receiver clock-based integrity monitoring for GPS precision approaches," *IEEE Transactions on Aerospace and Electronic Systems*, Vol. 42, Issue: 2, April 2006.
- [24] Kasdin, N. J., "Discrete simulation of colored noise and stochastic processes and $1/f^{\alpha}$ power law noise generation," *Proceedings of the IEEE*, Vol. 83, Issue 5, May 1995.
- [25] Lee, Y. C. and McLaughlin, M. P. "Feasibility Analysis of RAIM to Provide LPV-200 Approaches with Future GPS," *ION GNSS 20th International Technical Meeting of the Satellite Division*, Sep. 2007, Fort Worth, TX.
- [26] Blanch, J., Ene, A. Walter, T. and Enge P., "An Optimized Multiple Hypothesis RAIM Algorithm for Vertical Guidance," *ION GNSS 20th International Technical Meeting of the Satellite Division*, Sep. 2007, Fort Worth, TX.

APPENDIX

DERIVATION OF THE COVARIANCE OF STOCHASTIC CLOCK COASTING ERRORS USING IMPULSE RESPONSE MODEL

A power law model is typically used to model the power spectrum of clock fractional frequency measurements. The magnitude of power spectrum is proportional to $1/f^\alpha$, which has the form written below as:

$$\begin{aligned} S_y(f) &= h_2 f^2 + h_1 f + h_0 f^0 + h_{-1} f^{-1} + h_{-2} f^{-2} \\ &= s_{y_2}(f) + s_{y_1}(f) + s_{y_0}(f) + s_{y_{-1}}(f) + s_{y_{-2}}(f) \end{aligned} \quad (\text{a.1})$$

where the subscript y represents the clock fractional frequency conventionally and f is Fourier frequency in Hz.

As explained in the section on stochastic clock model, s_{y_0} , $s_{y_{-1}}$ and $s_{y_{-2}}$ are the dominant sources of random clock coasting errors. Each error source can be modeled as white noise passing through a transfer function in Laplace domain (' s ' domain), and its contribution to the random clock phase coasting error is the time integral of the resulted Laplace function:

$$\begin{aligned} n(s) &\rightarrow H_{y_i}(s) \rightarrow y_i(s) \rightarrow 1/s \rightarrow x_i(s) \\ \Rightarrow n(s) &\rightarrow H_{y_i}(s)/s \equiv H_{x_i}(s) \rightarrow x_i(s) \end{aligned} \quad (\text{a2})$$

where n is the white noise, H is the transfer function, y_i is the fractional frequency error corresponding to the s_{y_i} error source and the x_i is the resulting clock phase coasting error.

The transfer function $H_{y_i}(s)$ in Equation (a2) can be obtained by decomposing the corresponding term in the power law spectrum equation (Equation (a1)). The transfer functions for each dominant error sources can be derived as:

$$\begin{aligned} H_{y_0}(s) &= \sqrt{h_0/2} \Rightarrow H_{x_0}(s) = \sqrt{h_0/2s^2} \\ H_{y_{-1}}(s) &= \sqrt{\pi h_{-1}/s} \Rightarrow H_{x_{-1}}(s) = \sqrt{\pi h_{-1}/s^3} \\ H_{y_{-2}}(s) &= \sqrt{2\pi^2 h_{-2}/s^2} \Rightarrow H_{x_{-2}}(s) = \sqrt{2\pi^2 h_{-2}/s^4} \end{aligned} \quad (\text{a3})$$

The impulse-response functions for each error source can be derived by performing the inverse Laplace transform on each $H_{x_i}(s)$, and the time-response functions are the results of the convolution between the impulse response and the delta function ($\delta(t)$):

$$\begin{aligned} h_{x_0}(t) &= \sqrt{h_0/2} \Rightarrow x_0(t) = \int_0^t h_{x_0}(u) \delta(t-u) du \\ h_{x_{-1}}(t) &= 2\sqrt{h_{-1}t} \Rightarrow x_{-1}(t) = \int_0^t h_{x_{-1}}(u) \delta(t-u) du \\ h_{x_{-2}}(t) &= t\sqrt{2\pi^2 h_{-2}} \Rightarrow x_{-2}(t) = \int_0^t h_{x_{-2}}(u) \delta(t-u) du \end{aligned} \quad (\text{a4})$$

The time-response functions for random frequency deviation can be derived in the similar matter:

$$\begin{aligned} h_{y_0}(t) &= \sqrt{h_0/2} \delta(t) \Rightarrow y_0(t) = \int_0^t h_{y_0}(u) \delta(t-u) du \\ h_{y_{-1}}(t) &= \sqrt{h_{-1}/t} \Rightarrow y_{-1}(t) = \int_0^t h_{y_{-1}}(u) \delta(t-u) du \\ h_{y_{-2}}(t) &= \sqrt{2\pi^2 h_{-2}} \Rightarrow y_{-2}(t) = \int_0^t h_{y_{-2}}(u) \delta(t-u) du \end{aligned}$$

Due to the nature of the random frequency deviations, the instantaneous value and standard deviation of the random frequency deviation are difficult to handle (for example, white frequency noise has infinite bandwidth and therefore infinite instantaneous standard deviation) and is not useful for prediction. However, the long term trend of the random frequency deviation is a more valuable property for prediction. Therefore, the random frequency deviation state in the coasting error model is defined as an average random frequency deviation after a certain coasting period, instead of the instantaneous random frequency deviation. The following equation is used to define the random frequency deviation state:

$$b_{w1}(t) = \frac{1}{t} \int_0^t y_0(u) du + \frac{1}{t} \int_0^t y_{-1}(u) du + \frac{1}{t} \int_0^t y_{-2}(u) du$$

In other words, the random frequency deviation is the random coasting phase deviation divided by coasting time.

Recall the random states in Equation (1), the error contribution to the states from each error source can be broken down as:

$$b_{w0}(\Delta t) = x_0(\Delta t) + x_{-1}(\Delta t) + x_{-2}(\Delta t) \quad (\text{a5})$$

$$b_{w1}(\Delta t) = [x_0(\Delta t) + x_{-1}(\Delta t) + x_{-2}(\Delta t)] / \Delta t \quad (\text{a6})$$

The covariance of the random clock coasting error can now be derived as:

$$\begin{aligned} E([b_{w0} \quad b_{w1}]^T [b_{w0} \quad b_{w1}]) &= \begin{bmatrix} q_{11} & q_{12} \\ q_{21} & q_{22} \end{bmatrix} \\ &= E([(x_0(\Delta t) + x_{-1}(\Delta t) + x_{-2}(\Delta t)) \quad (x_0(\Delta t) + x_{-1}(\Delta t) + x_{-2}(\Delta t)) / \Delta t]^T \\ &\quad [(x_0(\Delta t) + x_{-1}(\Delta t) + x_{-2}(\Delta t)) \quad (x_0(\Delta t) + x_{-1}(\Delta t) + x_{-2}(\Delta t)) / \Delta t]) \end{aligned}$$

Because each error source is derived from the white noise model, the cross correlation between different error sources is zero. The elements of the resulted covariance are derived as:

$$q_{11}(\Delta t) = E[x_0(\Delta t)x_0(\Delta t)] + E[x_{-1}(\Delta t)x_{-1}(\Delta t)] + E[x_{-2}(\Delta t)x_{-2}(\Delta t)] \quad (\text{a7})$$

$$q_{22}(\Delta t) = E[x_0(\Delta t)x_0(\Delta t)]/\Delta t^2 + E[x_{-1}(\Delta t)x_{-1}(\Delta t)]/\Delta t^2 + E[x_{-2}(\Delta t)x_{-2}(\Delta t)]/\Delta t^2 = q_{11}(\Delta t)/\Delta t^2 \quad (\text{a8})$$

$$q_{12}(\Delta t) = q_{21}(\Delta t) = E[x_0(\Delta t)x_0(\Delta t)]/\Delta t + E[x_{-1}(\Delta t)x_{-1}(\Delta t)]/\Delta t + E[x_{-2}(\Delta t)x_{-2}(\Delta t)]/\Delta t = q_{11}(\Delta t)/\Delta t \quad (\text{a9})$$

The auto-correlation operation R_{xx} is defined as [6]:

$$\begin{aligned} R_{xx}(t_1, t_2) &\equiv E[x(t_1)x(t_2)] \\ &= E\left[\int_0^{t_1} h_x(u)\delta(t_1-u)du \int_0^{t_2} h_x(v)\delta(t_2-v)dv\right] \\ &= \int_0^{t_1} \int_0^{t_2} h_x(u)h_x(v)E[\delta(t_1-u)\delta(t_2-v)]dudv \\ &= \int_0^{t_1} \int_0^{t_2} h_x(u)h_x(v)R_\delta(u-v+t_2-t_1)dudv \end{aligned} \quad (\text{a10})$$

Let $t_1=t_2=\Delta t$, Equation (a10) can be simplified as:

$$\begin{aligned} R_{xx}(\Delta t) &\equiv E[x(\Delta t)x(\Delta t)] \\ &= \int_0^{\Delta t} \int_0^{\Delta t} h_x(u)h_x(v)R_\delta(u-v)dudv \end{aligned} \quad (\text{a11})$$

The elements of the covariance matrix for the random clock coating error can be re-written as:

$$q_{11}(\Delta t) = R_{x_0x_0}(\Delta t) + R_{x_{-1}x_{-1}}(\Delta t) + R_{x_{-2}x_{-2}}(\Delta t) \quad (\text{a12})$$

$$q_{22}(\Delta t) = (R_{x_0x_0}(\Delta t) + R_{x_{-1}x_{-1}}(\Delta t) + R_{x_{-2}x_{-2}}(\Delta t))/\Delta t^2 = q_{11}(\Delta t)/\Delta t^2 \quad (\text{a13})$$

$$q_{12}(\Delta t) = q_{21}(\Delta t) = (R_{x_0x_0}(\Delta t) + R_{x_{-1}x_{-1}}(\Delta t) + R_{x_{-2}x_{-2}}(\Delta t))/\Delta t = q_{11}(\Delta t)/\Delta t \quad (\text{a14})$$

Evaluating $R_{x_0x_0}$, $R_{x_{-1}x_{-1}}$ and $R_{x_{-2}x_{-2}}$ using Equation (a11), the analytical results are obtained as:

$$R_{x_0x_0}(\Delta t) = \int_0^{\Delta t} h_{x_0}(v)^2 dv = \frac{h_0}{2} \Delta t \quad (\text{a15})$$

$$R_{x_{-1}x_{-1}}(\Delta t) = \int_0^{\Delta t} h_{x_{-1}}(v)^2 dv = 2h_{-1}\Delta t^2 \quad (\text{a16})$$

$$R_{x_{-2}x_{-2}}(\Delta t) = \int_0^{\Delta t} h_{x_{-2}}(v)^2 dv = \frac{2\pi^2}{3} h_{-2}\Delta t^3 \quad (\text{a17})$$

Applying the above results into equations (a12) – (a14), the analytical relationships between the h coefficients and the covariance of random clock coating errors are derived and shown in Equation (1):

$$q_{11}(\Delta t) = \frac{h_0}{2} \Delta t + 2h_{-1}\Delta t^2 + \frac{2}{3}\pi^2 h_{-2}\Delta t^3$$

$$q_{22}(\Delta t) = \frac{h_0}{2\Delta t} + 2h_{-1} + \frac{2}{3}\pi^2 h_{-2}\Delta t$$

$$q_{12}(\Delta t) = q_{21}(\Delta t) = \frac{h_0}{2} + 2h_{-1}\Delta t + \frac{2}{3}\pi^2 h_{-2}\Delta t^2$$